Available online at www.sciencedirect.com
ScienceDirect
Journal of Bionic Engineering 14 (2017) 47–59

Design and Myoelectric Control of an Anthropomorphic Prosthetic Hand

Nianfeng Wang, Kunyi Lao, Xianmin Zhang

Guangdong Province Key Laboratory of Precision Equipment and Manufacturing Technology, *South China University of Technology*, *Guangzhou* 510640, *China*

Abstract

This paper presents an anthropomorphic prosthetic hand using flexure hinges, which is controlled by the surface electromyography (sEMG) signals from 2 electrodes only. The prosthetic hand has compact structure with 5 fingers and 4 Degree of Freedoms (DoFs) driven by 4 independent actuators. Helical springs are used as elastic joints and the joints of each finger are coupled by tendons. The myoelectric control system which can classify 8 prehensile hand gestures is built. Pattern recognition is employed where Mean Absolute Value (MAV), Variance (VAR), the fourth-order Autoregressive (AR) coefficient and Sample Entropy (SE) are chosen as the optimal feature set and Linear Discriminant Analysis (LDA) is utilized to reduce the dimension. A decision of hand gestures is generated by LDA classifier after the current projected feature set and the previous one are "pre-smoothed", and then the final decision is obtained when the current decision and previous decisions are "post-smoothed" from the decisions flow. The prosthetic hand can perform prehensile postures for activities of daily living and carry objects under the control of EMG signals.

Keywords: electromyography, anthropomorphic prosthetic hand, myoelectric control, pattern recognition, prehensile gestures

doi: 10.1016/S1672-6529(16)60377-3

1 Introduction

The anthropomorphic prosthetic hand is often mounted on an amputee and can be controlled by EMG. The sEMG signal is a noninvasive electrical biosignal which can represent the muscles activities. Myoelectric control has been widely used to control peripheral devices[1,2], especially prosthetic limb[3], through extracting the information from the sEMG and evaluating the contraction state of the muscles.

1.1 Multifunctional anthropomorphic prosthetic hand

The ideal prosthetic hand is supposed to be the same with the human hand in shape and features. According to the performance, the prosthetic hands can be divided into cosmetic hand, body-powered hand and EMG prosthetic hand. During the last decade, several multifunctional anthropomorphic prosthetic hands with EMG control have been developed by some companies and research institutions[4–12]. Underactuation[4], variable compliance couplings and module design are often adopted in the multi-DoF hands which have functions similar to the human hand. The i-Limb hand has five independently controlled fingers which is controlled by simple open and close signals from two electrodes[5]. Dalley *et al.* developed a hand with 16 joints driven by 5 independent actuators which provided 8 hand postures[6]. The Smarthand consists 5 fingers and 4 DoFs, with 40 sensors used for automatic control and feedback delivery[7]. The Southampton Remedi-Hand has 5 fingers and 6 DoFs, which are controlled by feedback control system with dynamic force sensors and piezo-resistive resistors[8]. The UB hand III is a humanoid robot hand which is based on an endoskeleton made of rigid links connected with elastic hinges, and is actuated by sheath routed tendons[9]. The HIT/DLR prosthetic hand has strong capability of self adaptation with multi sensors and 5 fingers actuated by 3 motors[10]. The hand with three articulated fingers driven by 4 DC motors through a special underactuated transmission was developed by Zollo *et al.*[11] The Fluidhand is actuated with flexible fluidic actuators which constitutes a new hybrid concept of an anthropomorphic five fingered hand and a three

Corresponding author: Nianfeng Wang
E-mail: menfwang@scut.edu.cn

jaw robotic gripper[12]. The hands mentioned above all have appearance and size similar to human hand and can perform prehensile postures for activities of daily living.

1.2 EMG pattern recognition method

To meet the increasing DoFs of prosthetic hands and provide more reliable and dexterous control[13], the pattern recognition method in a supervised way is widely used[14,15]. The fundamental preprocessing parts of the pattern recognition method includes data preprocessing, data windowing, feature extraction and classification[14]. The corresponding features are extracted from various muscle activities, and then the features are assigned to classes which represent relevant limb motions, that are the patterns. These patterns are learned by an algorithm which is then used to classify the limb motions[16]. The accuracy of the pattern recognition in sEMG greatly depends on the selection and extraction of features. A variety of EMG features has been used to represent the original EMG signals, which can be divided into 3 categories: time domain, frequency domain and time-frequency domain[1]. The time domain features are calculated from the time series of raw EMG signals. It has good classification property and enables simple calculation. Hudgins *et al.* used 5 time domain features including MAV, Mean Absolute Value Slope (MAVS), Zero Crossings (ZC), Slope Sign Changes (SSC) and Waveform Length (WL) to recognize 4 forearm motions and gained an average accuracy rate of 91%, which proved the effectiveness of time domain features[17]. Kim *et al.* successfully classified four wrist movements by using Integrated Absolute Value (IAV) and Root Mean Square (RMS)[18]. Features in frequency domain mainly reflect the fatigue of the muscle and the recruitment of motion unit, which usually contain Mean Frequency (MNF), Middle Frequency (MDF), Peak Frequency (PKF), Mean Power (MNP) and Total Power (TTP)[19]. However, Phinyomark *et al.* found that frequency domain features had worse performance than that in time domain when using MNF and MDF to recognize the hand gestures[20]. Features in time-frequency domain mainly contain Wavelet Packet Transform (WPT) and Short-time Fourier Transform (STFT), which can analyze signals in time domain and frequency domain at the same time though the calculation is complex. Englehart *et al.* used WPT and LDA to classify four kinds of hand and wrist motions and gained an average accuracy rate of 98%[21].

Due to the instability and stochasticity of sEMG signals, it is difficult for only one feature to represent the relevant hand gesture[22]. Therefore, feature set (the combination of different features) is often used to describe the sEMG signals[17,18,23–25]. However, high dimension feature vector will result in redundant data and classification burden. Principal Component Analysis (PCA)[26–29] and LDA are often used in dimension reduction[30,31]. Hargrove *et al.* obtained a higher classification accuracy when using individual PCA to preprocess raw EMG signals[29]. Chu *et al.* recognized nine movements of forearm, wrist and palm with 4 electrodes and obtained the accuracy of 97.4%, by utilizing LDA to reduce the dimension of the features extracted by WPT from 1024 to 8[8]. Khushaba *et al.* used LDA to reduce a series of features to the dimension of 9 and got the accuracy of 90% when recognizing 10 independent and associated motions of fingers[31].

Based on our previous research[32,33] on the off-line test and on-line recognition, an anthropomorphic prosthetic hand is presented and its myoelectric control system is built. MAV, VAR, the 4th AR and SE are selected as the optimal feature set, and LDA is utilized to reduce the dimension of the features. A combination of "pre-smoothing" and "post-smoothing" method makes the recognition of continuous gestures possible. A virtual hand is built to display the recognition result. All those compose the myoelectric control strategy of the EMG prosthetic hand to execute grasping tasks.

2 Prosthetic hand design

An anthropomorphic prosthetic hand (Fig. 1) is designed, which is made of aluminium alloy. The prosthetic hand has 5 fingers, 15 joints and 4 DoFs, with similar appearance and size to the human hand. The thumb and forefinger have independent movements, while the middle, ring and little fingers move

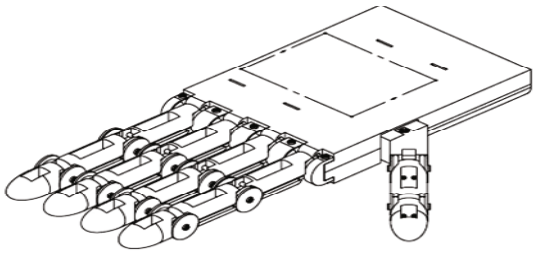

Fig. 1 The prosthetic hand.

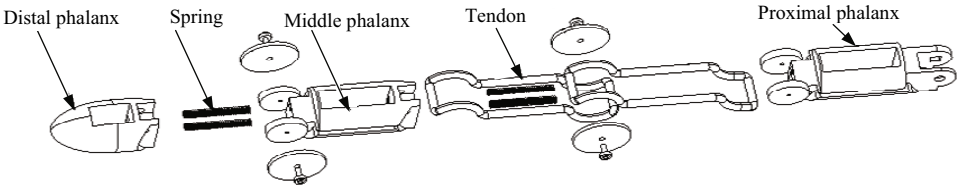

Fig. 2 The exploded view of the finger.

simultaneously. Each finger has a single DoF, as the movements of the distal and middle phalanxes (the thumb has only the distal phalanx) are coupled with the proximal phalanx. Flexure hinges are used to connect each phalanx as the finger joints. The prosthetic hand is actuated by 4 DC motors, which are settled in the palm. The prosthetic hand is light with compact structure.

2.1 Tendon driven finger

Module design is adopted that the forefinger, middle, ring and little fingers have the same structure. As shown in Fig. 2, the finger of the prosthetic hand has three phalanxes, proximal, middle and distal phalanx. Each phalanx is connected by 2 equal length extension springs placed side by side, which compose a flexure hinge. The tendons go through the phalanxes and drive the fingers to open or close by pulling or releasing the ropes.

Compliant mechanism is adopted in the joint design of the prosthetic hand. The joint will need only one positive actuator to ensure the basic motions like grasping, as additional tendons for finger extension are not necessary. When the finger flexes (Fig. 3), the extension spring will bend to a certain extent, having a relatively large displacement without any permanent deformation or torsion. In order to limit the transverse motion of the flexure hinge, two springs are set abreast in each joint.

Tendon-driven mechanisms are used for prosthetic hand transmissions. As show in Fig. 4, in the compliance coupling that the proximal joint moves following the palm joint, the tendon passes through the whole proximal phalanx and is fasten to both of the palm and middle phalanx. As the same, in the compliance coupling that the distal joint moves following the proximal joint, the tendon passes through the whole middle phalanx and is fasten to both of the proximal phalanx and distal phalanx. As a result, when the palm joint rotates, the proximal and distal joint will rotate the same angle under the action of the tendons.

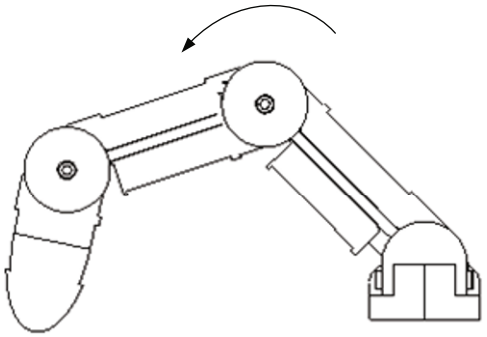

Fig. 3 The flexion of the finger.

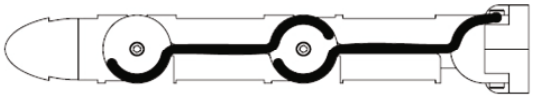

Fig. 4 The tendon route of the finger.

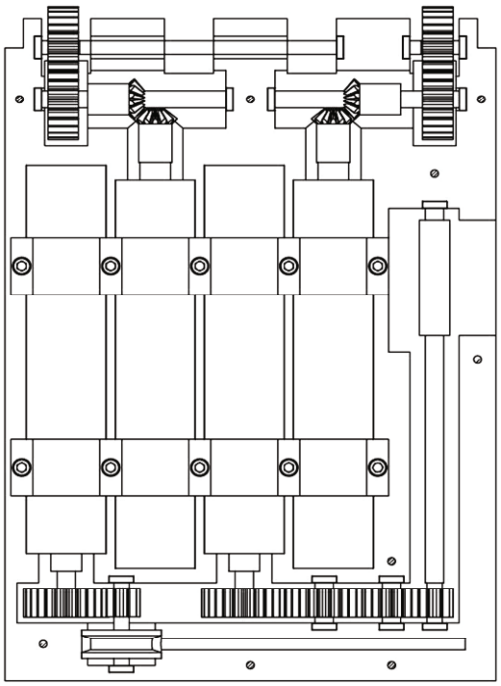

Fig. 5 The internal view of the palm.

2.2 Integrated palm

The EMG prosthetic hand is a highly integrated system with mechanical system, sensors, control and

driving system. As show in Fig. 5, the driving system of the prosthetic hand is set up inside the palm with 4 independent actuators in order to control 5 fingers with 4 DoFs including the rotation of the thumb around palm, the flexion and stretch of the thumb and forefinger, and the simultaneous movement of the middle, ring and little fingers. The driving mechanisms of the flexion and stretch motion of the forefinger and the simultaneous movement of the middle, ring and little fingers are the same that they are driven by an independent actuator respectively through a pair of bevel gears and a pair of cylindrical gears whose transmission ratio is 10:26. The rotation of the thumb is through a gear train of 4 cylindrical gears, and the flexion and stretch motion of the thumb is through a pair of cylindrical gears and a pulley which is fastened with a tendon. Their transmission ratio is 10:26.

2.3 Driving and control system

In order to control the 4 independent motors to rotate to the appropriate position so as to let the prosthetic hand finish the specified grasp tasks, the SPiiPlus NTM controller and the UDMlc motion driver from ACS Motion Control company are selected, and the matched software is SPiiPlus MMI Application Studio. The DC graphite brush micro motors from Maxon company are used as the motors for the prosthetic hand, and planetary gearboxes as the reducers for the micro motors. Encoders with 2 channels and line driver from Maxon company are adopted as the encoders for the micro motors.

Due to the transmission ratio of the rotation of the palm, proximal and distal joint is 1, the positional equation of the fingertip can be calculated as:

$$\begin{bmatrix} x \\ y \\ z \\ 1 \end{bmatrix} = \begin{bmatrix} c_{123} & -s_{123} & 0 & L_1c_1 + L_2c_{12} + L_3c_{123} \\ s_{123} & c_{123} & 0 & L_1s_1 + L_2s_{12} + L_3s_{123} \\ 0 & 0 & 1 & 0 \\ 0 & 0 & 0 & 1 \end{bmatrix} \begin{bmatrix} x_{\mathrm{P}} \\ y_{\mathrm{P}} \\ z_{\mathrm{P}} \\ 1 \end{bmatrix}, \quad (1)$$

where L_1, L_2 and L_3 are the length of the proximal, middle and distal phalanx, respectively. θ_1, θ_2 and θ_3 are the rotation angle of the palm, proximal and distal joint, respectively. $c_1 = \cos\theta_1$, $s_1 = \sin\theta_1$, $c_{12} = \cos(\theta_1 + \theta_2) = c_1c_2 - s_1s_2$, $s_{12} = \sin(\theta_1 + \theta_2) = c_1s_2 + s_1c_2$, *etc*. According to the position equation, the movement path and function space of the fingertip are shown in Fig. 6. Therefore, the prosthetic hand can be easily controlled to do the specified tasks by controlling the rotation angles of the 4 motors.

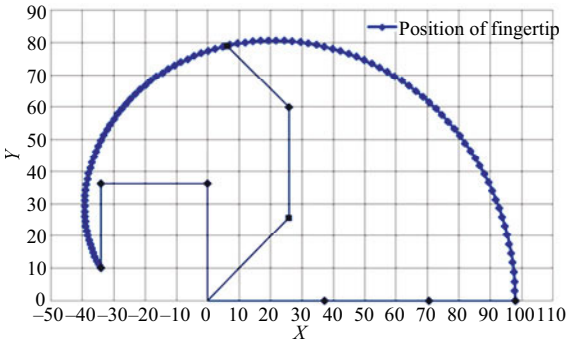

Fig. 6 The movement path and function space of the fingertip.

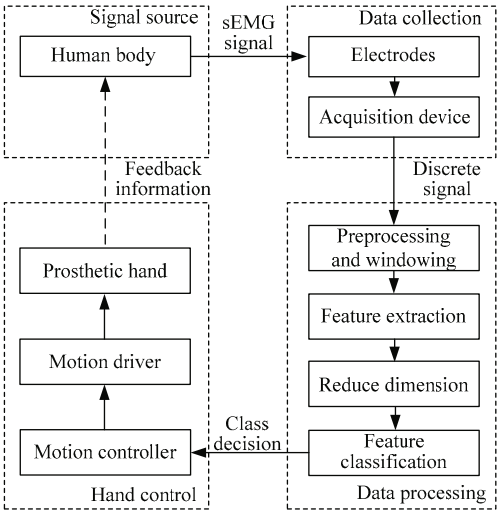

Fig. 7 The framework of the whole system.

3 Myoelectric control system

The myoelectric control system of the EMG prosthetic hand consists of 4 basic parts, signal source (the sEMG signals from the forearm of healthy subjects), data collection, data processing and prosthetic hand control. Fig. 7 shows the relations between each part. The sEMG signals are collected from 2 electrodes into acquisition device. The data processing part includes preprocessing and windowing, feature extraction, dimension reduction and feature classification. The final decision is sent to the motion controller and drives the prosthetic hand through motion driver.

3.1 Data collection

The eight prehensile hand gestures based on Taylor *et al.*[34] (Fig. 8) are designed to test the myoelectric control system and the hand design, which include

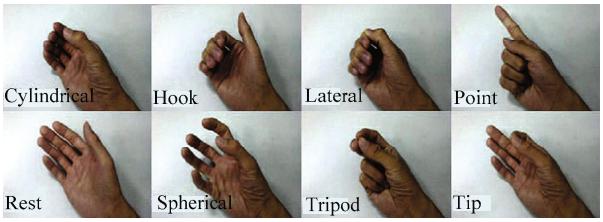

Fig. 8 Eight prehensile hand gestures.

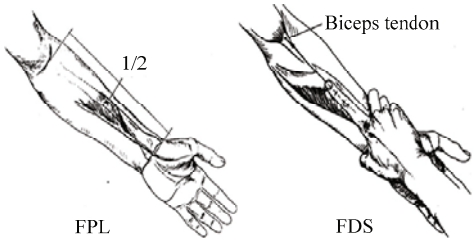

Fig. 9 The position of FPL and FDS[35].

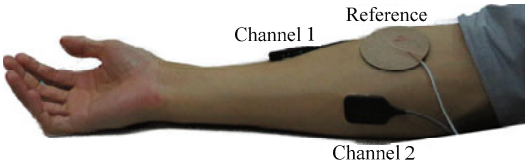

Fig. 10 The position of electrodes on the right forearm.

cylindrical, hook, lateral, point, rest, spherical, tripod and tip. These hand gestures can complete most grasp tasks in activities of daily living, whose main functions are described as:

(1) Cylindrical: For grasping cylindrical objects like a bottle or a glass.

(2) Hook: For carrying or pulling objects through four fingers, such as a briefcase.

(3) Lateral: For holding objects between the thumb and the lateral of the forefinger, such as a key or a card.

(4) Point: For showing directions or punching buttons.

(5) Rest: A platform posture for holding a plate or a book.

(6) Spherical: For grasping objects by the whole hand, such as a tennis ball.

(7) Tripod: For grasping small objects between the thumb, forefinger and the middle finger, such as a bottle cap.

(8) Tip: For pinching smaller objects like pins.

As these hand gestures mainly involve the flexion of both the thumb and the rest four fingers, the Flexor Pollicis Longus (FPL) and Flexor Digitorum Superficialis (FDS) (Fig. 9) are selected as the revelent muscles for the acquisition of sEMG signals. Two DE-2.1 differential EMG sensors (Delsys Inc., Boston, MA) are used to collect the sEMG signals and placed above the corresponding muscles, respectively. The sEMG signals are sampled at 1000Hz per channel with the acquisition device (National Instruments, PCI-6220). A Labview Virtual Instrument (VI) is developed for collecting, displaying and storing the sEMG signals for further processing.

Five male subjects and one female subject who are able-bodied with no neurological or muscular disorders participate in the experiments. First of all, the skin preparation is conducted to reduce the impedance between the electrode and skin, which includes removing the hair, scrubbing the skin and cleaning the skin with water[36]. Then, the two electrodes are placed on the skin above FPL and FDS shown in Fig. 10. Before the experiment, each subject is given half an hour to practice the series of the hand gestures until he or she is familiar with them and the contractions are considered repeatable. At the same time, the sEMG signals are observed to check the contact condition between the electrodes and the skin and guarantee high Signal Noise Ratio (SNR).

3.2 Feature extraction

When segmenting the raw sEMG signals, the overlapping windowing scheme is used. Fig. 11 shows the difference between overlapping windowing scheme and nonoverlapping windowing scheme. The time from the onset of muscle contraction until the system generates a corresponding class decision should be less then 300ms[37]. Due to the nonstationarity of sEMG signals, it is very difficult for one window to generate the correct decision. One possible solution is to obtain as many decisions as possible and to smooth these decisions to get the final decision. The overlapping windowing scheme can solve the problems. The number of windows can be calculated as:

$$No.\ of\ windows = \frac{data\ length - window\ size}{window\ increment} + 1, \quad (2)$$

The window length is defined as 250ms[38] and the increment is 70ms in this paper.

The raw sEMG signal is not suitable for classification, as it has large quantity of data and redundant information, which will burden the classifier and reduce recognition rate. A set of appropriate features is needed

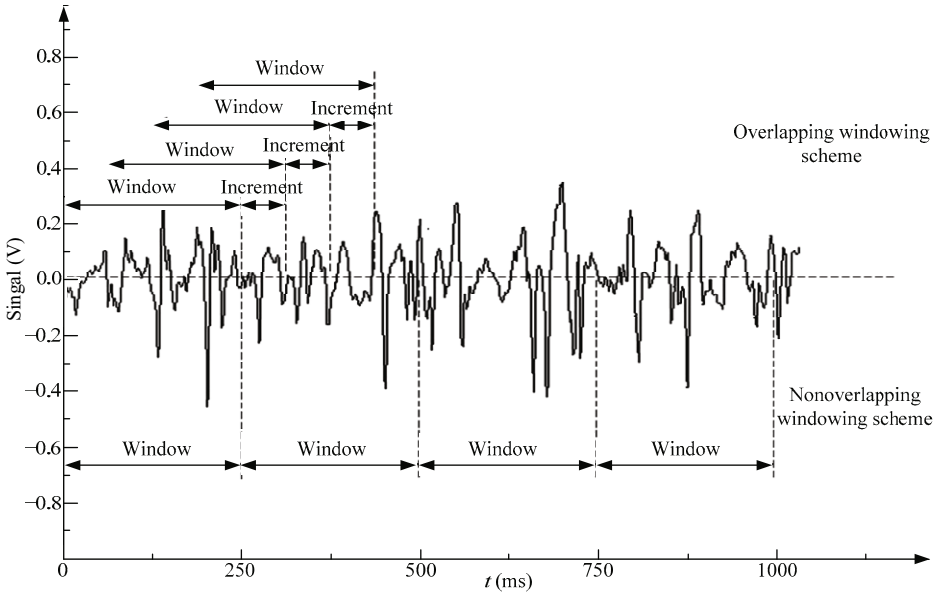

Fig. 11 The comparison of overlapping and nonoverlapping windowing scheme.

to represent the classification information of the gestures. According to our previous research, the optimal feature set for the recognition system includes MAV, VAR, the 4th AR and SE. MAV[19] equals the mean of absolute value of sEMG signal amplitude in a window. $s(i)$ $\{1 \le i \le N\}$ is used to denote the i-th point in a sEMG window. N is the length of the window. Therefore, MAV can be calculated as:

$$MAV = \frac{1}{N}\sum_{i=1}^{N}|s(i)|. \tag{3}$$

VAR[19] is calculated by squaring the differences between each value of sEMG signals in a window and the mean, and diving the sum of the squares by the length of the window. As the mean of the sEMG signals is supposed to be zero, VAR of the sEMG signals can be obtained by:

$$VAR = \frac{1}{N-1}\sum_{i=1}^{N}s(i)^2, \tag{4}$$

The 4th AR[19] is a time series model of sEMG signals. When fitting the auto-regressive model to a sEMG window, $s(i)$ can be expressed by:

$$s(i) = w(i) + \sum_{k=1}^{P}a_k s(i-p), \tag{5}$$

where p is the model order ($p = 4$), a_k is AR coefficients and $w(i)$ is the residual white noise. SE[19] is a single robust feature, which can be calculated as[39]:

(1) For a certain sEMG window $s(i)$ $\{1 \le i \le N\}$, form $N - n + 1$ vectors:

$$\boldsymbol{x}_n(j), (1 \le j \le N-n+1), \tag{6}$$

where $\boldsymbol{x}_n(j)$ is the n-dimension vector of data points from $s(j)$ to $s(j + n - 1)$.

(2) The distance between $\boldsymbol{x}(j)$ and $\boldsymbol{x}(k)$ is defined as:

$$d[\boldsymbol{x}_n(j), \boldsymbol{x}_n(k)] = \max\{|s(j+h) - s(k+h)|\} \quad (1 \le h \le N-1,\ j \ne k), \tag{7}$$

(3) For every $\boldsymbol{x}_n(j)$, if the distance $d[\boldsymbol{x}(j), \boldsymbol{x}(k)]$ is less than the given tolerance r, increase the counter $N^n(j)$ by one.

Define the function:

$$B^n(r) = (N-n+1)^{-1}\sum_{j=1}^{N-n+1}\frac{N^n(j)}{N-n}. \tag{8}$$

(4) Similarly, calculate the

$$B^{n+1}(r) = (N-n)^{-1}\sum_{j=1}^{N-n}\frac{N^{n+1}(j)}{N-n-1}. \tag{9}$$

(5) Therefore, SE can be obtained by:

$$SE(n, r, N) = -\ln\frac{B^{n+1}(r)}{B^n(r)}, \tag{10}$$

The specific parameters for SE are the dimension n and tolerance r. n is set as 2 and r is set as $0.25 \times \sigma$ in this paper. σ is the standard deviation of the sEMG signals in

each analysis window, respectively.

3.3 Dimension reduction

It will increase the burden of classifier and the recognition time if the feature vector is directly fed into the classifier. Hence, feature reduction is necessary. LDA algorithm is used to reduce the feature dimension.

The basic idea of LDA is to seek a projection matrix $\boldsymbol{W}$ which projects the original dataset into a new coordinate system where the class separability is maximized by making the between-class scatter ($\boldsymbol{S}_b$) largest and the within-class scatter ($\boldsymbol{S}_w$) smallest[28].

Before projected, the mean vector for each class is defined to be:

$$\boldsymbol{\mu}_i = \frac{1}{N_i}\sum_{j=1}^{N_i}\boldsymbol{x}_j, \tag{11}$$

where N_i is the number of samples of each class, and $\boldsymbol{x}_j$ denotes the original feature vectors of each class. Then, the projected mean vector can be calculated as:

$$\tilde{\boldsymbol{u}}_i = \boldsymbol{W}^{\mathrm{T}}\boldsymbol{\mu}_i, \tag{12}$$

For the between-class scatter ($\boldsymbol{S}_b$), the distance between the mean vector for each class $\boldsymbol{\mu}_i$ and the mean vector for all classes $\boldsymbol{\mu}$ is:

$$L = \boldsymbol{W}^{\mathrm{T}}\left[\sum_{i=1}^{C}(\boldsymbol{\mu}_i-\boldsymbol{\mu})(\boldsymbol{\mu}_i-\boldsymbol{\mu})^{\mathrm{T}}\right]\boldsymbol{W}, \tag{13}$$

where $\boldsymbol{S}_b$ is defined as:

$$\boldsymbol{S}_b = \sum_{i=1}^{C}N_i(\boldsymbol{\mu}_i-\boldsymbol{\mu})(\boldsymbol{\mu}_i-\boldsymbol{\mu})^{\mathrm{T}}, \tag{14}$$

For the within-class scatter $\boldsymbol{S}_w$, the variance of dataset of each class is:

$$\boldsymbol{S}_i = \boldsymbol{W}^{\mathrm{T}}\left[\sum_{j=1}^{N_i}(\boldsymbol{x}_j-\boldsymbol{\mu})(\boldsymbol{x}_j-\boldsymbol{\mu})^{\mathrm{T}}\right]\boldsymbol{W}, \tag{15}$$

Then the sum of $\boldsymbol{S}_i$ is:

$$\sum_{i=1}^{C}\boldsymbol{S}_i = \boldsymbol{W}^{\mathrm{T}}\sum_{i=1}^{C}\left[\sum_{j=1}^{N_i}(\boldsymbol{x}_j-\boldsymbol{\mu})(\boldsymbol{x}_j-\boldsymbol{\mu})^{\mathrm{T}}\right]\boldsymbol{W}, \tag{16}$$

$\boldsymbol{S}_w$ is defined as:

$$\boldsymbol{S}_w = \sum_{i=1}^{C}\sum_{j=1}^{N_i}(\boldsymbol{x}_j-\boldsymbol{\mu})(\boldsymbol{x}_j-\boldsymbol{\mu})^{\mathrm{T}}, \tag{17}$$

where C is the number of class. And the optimal projection matrix $\boldsymbol{W}$ can be obtained by:

$$J(\boldsymbol{W}) = \frac{\det(\boldsymbol{W}^{\mathrm{T}}\boldsymbol{S}_b\boldsymbol{W})}{\det(\boldsymbol{W}^{\mathrm{T}}\boldsymbol{S}_w\boldsymbol{W})}, \tag{18}$$

Then the original feature matrix ($M \times N$) is projected by:

$$\boldsymbol{y} = \boldsymbol{W}^{\mathrm{T}}\boldsymbol{x}, \tag{19}$$

The matrix $\boldsymbol{y}$ stands for the projected feature vectors with R-dimensionality ($R \le M$, $R \le C-1$), where M is the dimension of original feature vectors and C is the number of categories. To obtain the best recognition accuracy, the proper value for R is 7.

3.4 Feature classification

Half of the samples of each hand gesture are used for training, which can be represented by 14-dimension feature vectors after feature extraction. In order to observe the distribution of Projected Feature Vectors (PFVs), R is chosen as 3. After dimension reduction, the distribution of PFVs is shown in Fig. 12. The black dots which are in the middle of the PFVs of each hand gesture in Fig. 12 are the averages of the PFVs of the hand gestures, named label dots. It can be found that the most PFVs of each hand gesture are obviously around its corresponding label dots, though some individual PFVs deviated from it seriously. So the label dots represent the position information of each hand gesture that the LDA algorithm can be used in classification. When the PFV of a test sample is sent into the LDA classifier, it is compared with the label dots of each hand gesture and the decision of hand gestures is obtained according to the distance between the PFV and the label dots.

4. Experiments and results

4.1 Off-line recognition

As the data collection scheme mentioned in

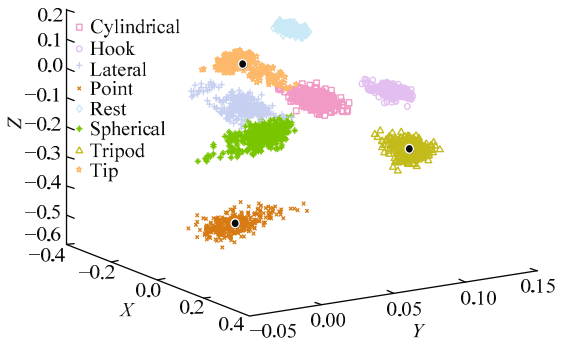

Fig. 12 The distribution of PFVs.

section **3.1**, the off-line recognition signals are collected by the Bagnoli-4 EMG System (Delsys Inc., Boston, MA). When the subjects make hand gestures and hold 5 seconds during each contraction, 5000 data points are acquired. Since a step voltage exists at the very beginning of sEMG signals due to the settings of the Data Acquisition Card, the first 250 data points are removed to avoid the influence. After segmenting the data points by the overlapping windowing scheme, 65 windows are obtained during each contraction. So there are 650 (65 × 10) samples for each hand gesture, the first 325 of which are used for training and the rest are for off-line testing. During the off-line training, the feature set including MAV, VAR, the 4th AR and SE is extracted from each window, generating 2600 (325 × 8) feature vectors which are 14-dimension in total. Then the dimension reduction through LDA algorithm is conducted. The 14-dimension feature vectors are projected into 7-dimension, generating a projection matrix $\boldsymbol{W}$ and label dots matrix $\boldsymbol{P}$ which is the mean values of PFVs from each hand gesture and represents different hand gestures. During the off-line testing, the later 325 samples of each hand gesture are projected by the projection matrix $\boldsymbol{W}$ after feature extraction, generating 7-dimension PFVs. Each PFV is compared with the label dots of each hand gesture in the matrix $\boldsymbol{P}$ to obtain the decision of hand gestures. Figs. 13 and 14 show the flowchart and facility of the off-line training.

In the off-line training system, the sEMG signals of 8 hand gestures of 6 subjects are acquired. The subjects are instructed by the hand gestures shown on the screen to elicit a corresponding contraction and hold for 5 seconds. Every hand gesture is repeated 10 times with a resting time of 6 seconds between each contraction. Once a hand gesture with 10 repetitions is finished, the subjects have 5 minutes for rest to avoid muscle fatigue before the next hand gesture. In the dimension reduction part, LDA algorithm is used and the optimal value of R is the largest value in the available range which retains the most information of different hand gestures and achieves the best accuracy. The LDA classifier is also utilized in the feature classification part. In the off-line recognition, "pre-smoothing" is used to average the current PFV and the previous PFV before the classification. This method improves the average accuracy rate of each hand gesture from 95.94% to 98.12%, and the stand deviation of each hand gesture is less than 6%.

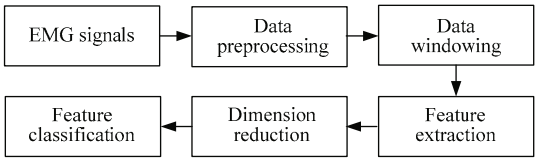

Fig. 13 Flowchart of the off-line training.

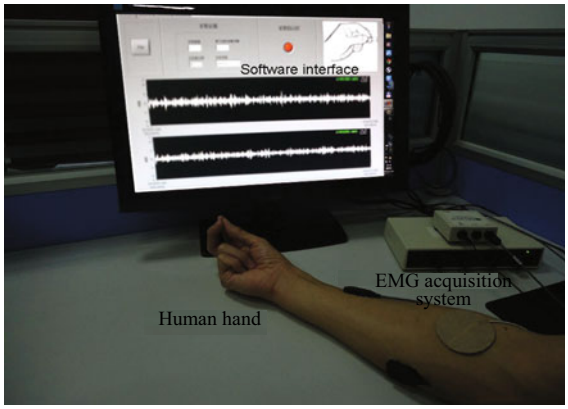

Fig. 14 Facility of the off-line training.

Compared with the original feature set including MAV, VAR and the 4th AR, the optimal feature set can raise the off-line average accuracy rate form 98.12% to 99.04%, and decrease the standard deviation from 1.69% to 0.65%.

4.2 On-line recognition

After the subjects finish the off-line training, they are tested by the on-line realtime recognition. An effective realtime recognition system should meet the requirements of accuracy rate and time delay limitation. Therefore, a combination of "pre-smoothing" and "post-smoothing" is applied to realize the realtime recognition. The "pre-smoothing" is a smoothing process before the classification, which averages the current projected sample produced from the relevant window and the previous n projected samples to avoid a lengthy delay. The "post-smoothing" is a process of smoothing the decisions flow after the classification and gets the final decision. Each window will yield a decision during the increment assuming that the processing can take place while new data are being acquired. For a certain window, the current decision and the previous m decisions are compared, and the final decision is the one that occurs most often among the $m + 1$ decisions. If two decisions are equal, then the later decision in the decisions flow is taken as the final decision. On the basis of test, every 2 projected samples are averaged ($n = 1$) in the

"pre-smoothing" and the best value of *m* is defined as 12 in the "post-smoothing".

The flowchart of realtime recognition is shown in Fig. 15. During the realtime recognition, the myoelectric control system collects the sEMG signals from the forearm of the subjects continuously, performs the data windowing, feature extraction, dimension reduction, "pre-smoothing" and "post-smoothing", and generates a final decision every window increment (70 ms), until the user interrupt the program.

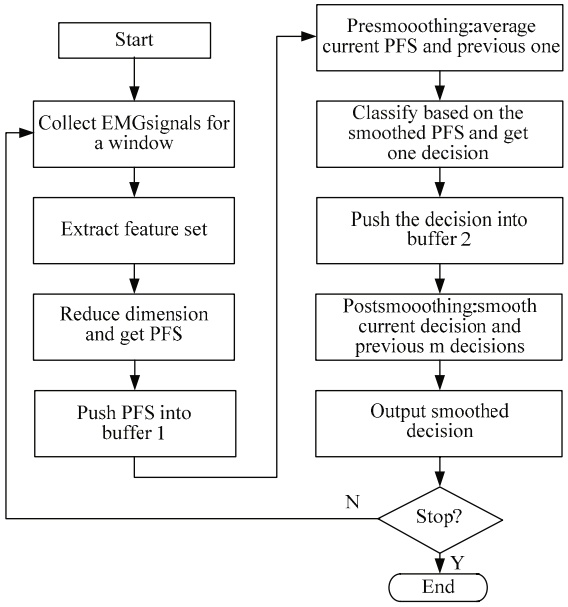

Fig. 15 Flowchart of the realtime recognition.

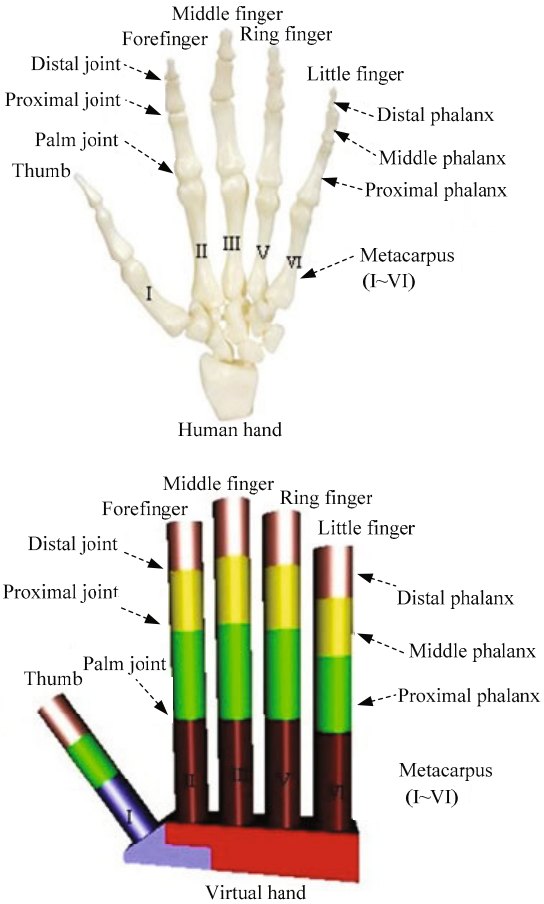

Fig. 16 The skeletons and joints of human hand and virtual hand.

In the on-line test, a virtual hand is shown on the screen to display the recognition result. Each subject is required to perform each hand gesture for 10 seconds in the following order: cylindrical, hook, lateral, point, rest, spherical, tripod and tip. Between every two hand gestures, the subjects are given 1 minute to rest. That is, the rest gesture is inserted into every two hand gestures. As expected, the average accuracy rate for all the subjects is consistently high. The method of "post-smoothing" using majority vote improves the on-line average accuracy rate to 97.35%. This scheme can also achieve high accuracy rate when the subject performs the hand gestures in a random order which does not have to perform the rest gesture between two different gestures. When some subjects participate in the experiment for the first time, the accuracy rate is much lower compared to their off-line training result for lack of sufficient training. However, it is anticipated that the on-line accuracy rate can be much closer to the off-line accuracy rate after a large number of training.

4.3 Virtual hand

In order to display the on-line recognition result visually, a virtual hand is developed using Virtual Reality Modeling Language (VRML). The virtual hand has 5 fingers with 19 DoFs, which has appearance similar to the skeleton of human hand which is shown in Fig. 16. The fingers flex when the angle values of the joints changes. So that, through adjusting the joints to the proper rotate angles, the virtual hand can be controlled to do the 8 hand gestures (Fig. 17). Therefore, the

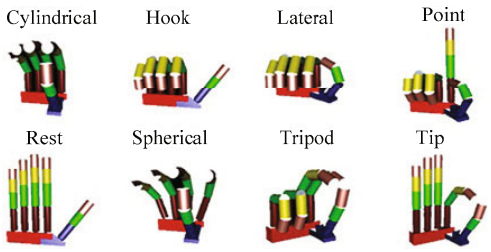

Fig. 17 The virtual hand gestures.

myoelectric control system of the prosthetic hand can be examined by the virtual hand.

A human hand can perform these gestures in a random order and the fingers move in a nature way. Therefore, a control strategy was proposed to make the virtual hand move naturally. First, the target angle values of all knuckles for each gesture were set. Second, when a final decision x was sent into the controller, the algorithm would calculate the total difference between the current knuckle values and the target ones. To make full use of decisions flow, the difference was divided into n_x parts equally. For a certain x, only one of the n_x parts was used to drive the virtual hand if its value was bigger than the threshold and n_x was bigger than 1. And then, the value of n_x decreased by 1 and the current knuckle values were updated in each loop. The initial value of n_x was set as 10 in this paper. The subscript x in n_x denotes from 1 to 8. Therefore, for each gesture, the virtual hand would take 10 steps to reach the target knuckle values from current ones. The threshold was set as 0 to make sure that n_x can be reset as 10 when the virtual hand had reached the target knuckle values. Fig. 18 showed the flowchart of driving the virtual hand.

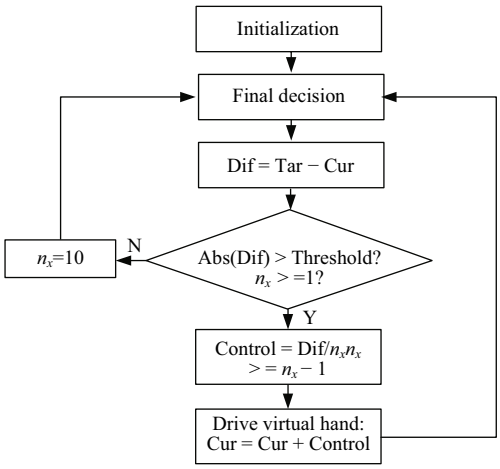

Fig. 18 The flowchart of driving the virtual hand.

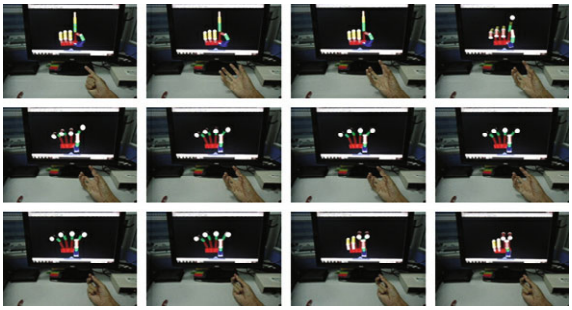

Fig. 19 The movement of the virtual hand.

Fig. 19 shows the movement of the virtual hand. In the experiment, the subject switches the hand gestures continuously in the order of point, spherical and tripod. The virtual hand moves following the human hand under the control of sEMG signals.

4.4 Prosthetic hand

The prototype of the prosthetic hand is shown in Fig. 20. The prosthetic hand can meet the requirements of cosmetic appearance and the grasp tasks in daily living. The shape and size of the prosthetic hand are similar to the human hand. Because the palm joints lack the DoF of swing, the prosthetic hand cannot achieve the spherical gesture. Therefore, the spherical gesture is defined the same as cylindrical gesture. As mentioned in section **2.3**, the prosthetic hand can achieve the 8 hand gestures by simply controlling the motors to rotate to the specified angles. Fig. 21 shows the 8 hand gestures of the prothetic hand when gasping objects.

Fig. 22 shows the overall system of the experiment. The control system consists of SPiiPlus NTM motion controller, UDMlc motion driver, and the matched software SPiiPlus MMI Application Studio from ACS Motion Control Company. The control programming of the motors is host-based, where the Labview Virtual Instrument is adopted to combine the myoelectric control system and the motor control system, through calling the

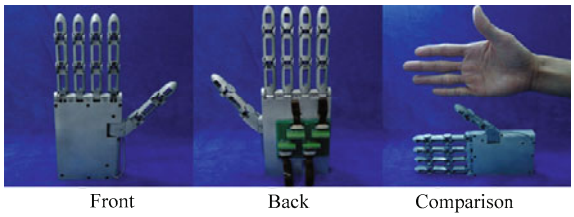

Fig. 20 The prototype of the prosthetic hand.

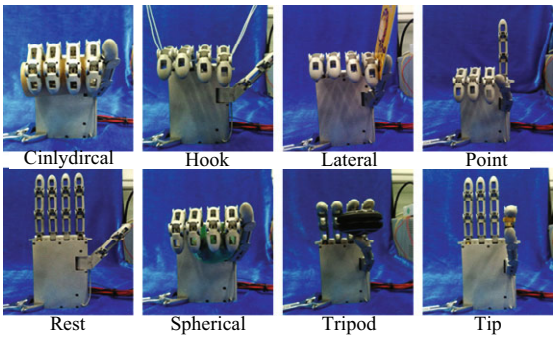

Fig. 21 The prosthetic hand gestures.

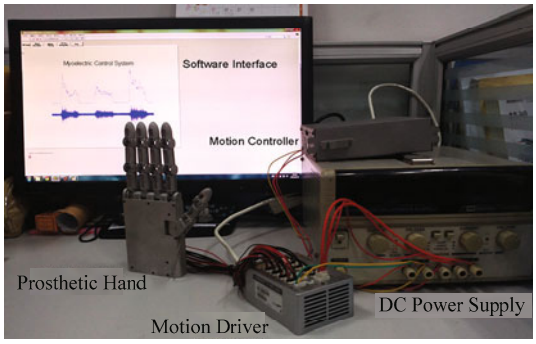

Fig. 22 The overall system.

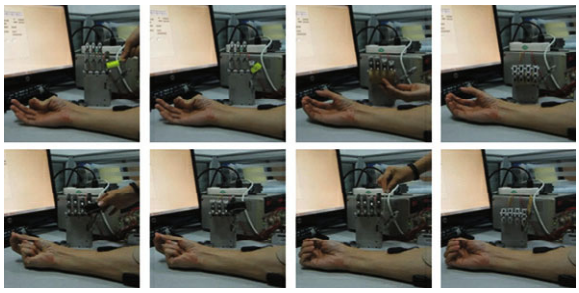

Fig. 23 The movement of the prosthetic hand.

functions from the Component Object Model (COM) lib to control the motors. There are 3 basic parts in the control program of the prosthetic hand including activating the specified motors, getting current position of the motors, and driving the motors to the designated position. In the on-line recognition system, the final decision of the hand gestures is generated every 70 ms. However, the motors can not finish a hand gesture command all the time in every 70 ms when the prosthetic hand is moving. Hence, the motion controller will stop the motors and get the error message when the commands are crowded. To solve the problem, the control system reads the hand gesture command every 500 ms. Fig. 23 shows the movement of the prosthetic hand controlled by the EMG signals in real time. From the experimental results, we showed that the proposed method is applicable for realtime myoelectric hand control without a perceived operation time delay.

5 Conclusion

In this paper, an anthropomorphic prosthetic hand using flexure hinge is designed, which is under the control of a realtime myoelectric control system using only 2 electrodes and classifying 8 hand gestures. The prosthetic hand consists of 5 fingers with 4 DoFs driven by 4 independent actuators. The phalanxes are connected by helical springs which make the joints elastic linkages. The movement of each joint is combined by coupled mechanism with tendons. All the 4 actuators are integrated in the palm which simplifies the design of the prosthetic hand. As a result, the hand is designed with cosmetic appearance and shape similar to human hand, which can accomplish most grasping tasks in the daily living. Pattern recognition is adopted in the myoelectric control system. MAV, VAR, the 4th AR and SE are selected as the optimal feature set, and the dimension is reduced by LDA algorithm. The “pre-smoothed” and “post-smoothed” are combined to smooth the output in the on-line recognition. Using the proposed method, we have recognized the 8 hand gesture from 2 channel EMG signals and controlled the prosthetic hand in real time. From the experiment, the prosthetic hand can grasp the objects by the control of EMG signals. In the future, the force feedback system will be added into the prosthetic hand to complete the whole system. Also, the relationship between the force level of contraction and the recognition accuracy rate will be explored.

Acknowledgment

This work is supported by National Natural Science Foundation of China (Grant Nos. 51575187 and 91223201), Science and Technology Program of Guangzhou (Grant No. 2014Y2-00217), Science and Technology Major Project of Huangpu District of Guang-Zhou (Grant No. 20150000661), the Fundamental Research Funds for the Central University (Grant No. 2015ZZ007) and Natural Science Foundation of Guangdong Province (Grant No. S2013030013355).

References

[1] Asghari O M, Hu H. Myoelectric control systems: A survey. *Biomedical Signal Processing and Control*, 2007, **2**, 275–294.

[2] Chan C C, Liao W H. Temporal gait parameters captured by surface electromyography measurement. *Proceedings of* 2012 *IEEE International Conference on Robotics and Biomimetics*, Guangzhou, China, 2012, 1056–1061.

[3] Cannan J, Hu H S. *Human-Machine Interaction* (*HMI*): *A Survey*, Technical Report CES-508, University of Essex, Colchester, UK, 2011.

[4] Chen W R, Xiong C H. On adaptive grasp with underactuated anthropomorphic hands. *Journal of Bionic Engineering*, 2016, **13**, 59–72.

[5] Connolly C. Prosthetic hands from touch bionics. *Industrial Robot*: *An International Journal*, 2008, **35**, 290–293.

[6] Dalley S, Wiste T, Withrow T, Goldfarb M. Design of a multifunctional anthropomorphic prosthetic hand with extrinsic actuation. *IEEE/ASME Transactions on Mechatronics*, 2009, **14**, 699–706.

[7] Cipriani C, Controzzi M, Carrozza M. The smarthand transradial prosthesis. *Journal of Neuroengineering and Rehabilitation*, 2011, **8**, 29–42.

[8] Zecca M, Micera S, Carrozza M C, Dario P. Control of multifunctional prosthetic hands by processing the electromyographic signal. *Critical Reviews in Biomedical Engineering*, 2002, **30**, 459–485.

[9] Lotti F, Tiezzi P, Vassura G, Biagiotti L, Palli G, Melchiorri C. Development of UB hand 3: Early results. *Proceedings of IEEE International Conference on Robotics and Automation*, Barcelona, Spain, 2005, 4488–4493.

[10] Huang H, Jiang L, Liu Y, Hou L, Cai H, Liu H. The mechanical design and experiments of hit/dlr prosthetic hand. *Proceedings of IEEE International Conference on Robotics and Biomimetics*, Kunming, China, 2006, 896–901.

[11] Zollo L, Roccella S, Guglielmelli E, Carrozza M, Dario P. Biomechatronic design and control of an anthropomorphic artificial hand for prosthetic and robotic applications. *IEEE/ASME Transactions on Mechatronics*, 2007, **12**, 418–429.

[12] Gaiser I, Pylatiuk C, Schulz S, Kargov A, Oberle R, Werner T. The fluidhand iii: A multifunctional prosthetic hand. *Journal of Prosthetics and Orthotics*, 2009, **21**, 91–96.

[13] Xu Z J, Tian Y T, Li Y. sEMG pattern recognition of muscle force of upper arm for intelligent bionic limb control. *Journal of Bionic Engineering*, 2015, **12**, 316–323.

[14] Scheme E, Englehart K. Electromyogram pattern recognition for control of powered upper-limb prostheses: State of the art and challenges for clinical use. *Journal of Rehabilitation Research and Development*, 2011, **48**, 643–659.

[15] Kent B A, Lavery J, Engeberg E D. Anthropomorphic control of a dexterous artificial hand via task dependent temporally synchronized synergies. *Journal of Bionic Engineering*, 2014, **11**, 236–248.

[16] Lorrain T, Jiang N, Farina D. Influence of the training set on the accuracy of surface emg classification in dynamic contractions for the control of multifunction prostheses. *Journal of Rehabilitation Research and Development*, 2011, **8**, 25.

[17] Hudgins B, Parker P, Scott R N. A new strategy for multifunction myoelectric control. *IEEE Transactions on Biomedical Engineering*, 1993, **40**, 82–94.

[18] Kim K S, Choi H H, Moon C S, Mun C W. Comparison of k-nearest neighbor, quadratic discriminant and linear discriminant analysis in classification of electromyogram signals based on the wrist-motion directions. *Current Applied Physics*, 2011, **11**, 740–745.

[19] Phinyomark A, Phukpattaranont P, Limsakul C. Feature reduction and selection for EMG signal classification. *Expert Systems with Applications*, 2012, **39**, 7420–7431.

[20] Phinyomark A, Hirunviriya S, Limsakul C, Phukpattaranont P. Evaluation of EMG feature extraction for hand movement recognition based on euclidean distance and standard deviation. *Proceedings of the* 2010 *ECTI International Conference on Electrical Engineering, Electronics, Computer, Telecommunications and Information Technology*, Chiang Mai, Thailand, 2010, 856–860.

[21] Englehart K, Hudgins B, Parker P A. A wavelet-based continuous classification scheme for multifunction myoelectric control. *IEEE Transactions on Biomedical Engineering*, 2001, **48**, 302–311.

[22] Park S H, Lee S P. Emg pattern recognition based on artificial intelligence techniques. *IEEE Transactions on Rehabilitation Engineering*, 1998, **6**, 400–405.

[23] Khushaba R N, Kodagoda S, Takruri M, Dissanayake G. Toward improved control of prosthetic fingers using surface electromyogram (EMG) signals. *Expert Systems with Applications*, 2012, **39**, 10731–10738.

[24] Chen X, Wang Z J. Pattern recognition of number gestures based on a wireless surface EMG system. *Biomedical Signal Processing and Control*, 2012, **8**, 184–192.

[25] Liu Y H, Huang H P, Weng C H. Recognition of electromyographic signals using cascaded kernel learning machine. *IEEE/ASME Transactions on Mechatronics*, 2007, **12**, 253–264.

[26] Jolliffe I. *Principal Component Analysis*, Wiley Online Library, USA, 2005.

[27] Artemiadis P K, Kyriakopoulos K J. EMG-based control of a robot arm using low-dimensional embeddings. *IEEE Transactions on Robotics*, 2010, **26**, 393–398.

[28] Chu J U, Moon I, Kim S K, Mun M S. Control of multifunction myoelectric hand using a real-time EMG pattern recognition. *Proceedings of* 2005 *IEEE/RSJ International Conference on Intelligent Robots and Systems*, Edmonton, Canada, 2005, 3511–3516.

[29] Hargrove L J, Li G, Englehart K B, Hudgins B S. Principal components analysis preprocessing for improved classification accuracies in pattern-recognition-based myoelectric control. *IEEE Transactions on Biomedical Engineering*, 2009, **56**, 1407–1414.

[30] Chu J U, Moon I, Lee Y J, Kim S K, Mun M S. A supervised

feature-projection-based real-time EMG pattern recognition for multifunction myoelectric hand control. *IEEE/ASME Transactions on Mechatronics*, 2007, **12**, 282–290.

[31] Khushaba R N, Kodagoda S, Takruri M, Dissanayake G. Toward improved control of prosthetic fingers using surface electromyogram (EMG) signals. *Expert Systems with Applications*, 2012, **39**, 10731–10738.

[32] Wang N F, Chen Y L, Zhang X M. The recognition of multi-finger prehensile postures using LDA. *Biomedical Signal Processing and Control*, 2013, **8**, 706–712.

[33] Wang N F, Chen Y L, Zhang X M. Realtime recognition of multi-finger prehensile gestures. *Biomedical Signal Processing and Control*, 2015, **13**, 262–269.

[34] Taylor C L, Schwarz R J. The anatomy and mechanics of the human hand. *Artificial Limbs*, 1955, **2**, 22–35.

[35] Lu Z. *Practical Electromyography*, People's Medical Publishing House, Beijing, China, 2000. (in Chinese)

[36] Konrad P. *The ABC of EMG: A Practical Introduction to Kinesiological Electromyography*, 1st ed, Noraxon U.S.A. Inc., Scottsdale, USA, 2005.

[37] Englehart K, Hudgins B. A robust, real-time control scheme for multifunction myoelectric control. *IEEE Transactions on Biomedical Engineering*, 2003, **50**, 848–854.

[38] Smith L H, Hargrove L J, Lock B A, Kuiken T A. Determining the optimal window length for pattern recognition-based myoelectric control: Balancing the competing effects of classification error and controller delay. *IEEE Transactions on Neural Systems and Rehabilitation Engineering*, 2011, **19**, 186–192.

[39] Richman J S, Moorman J R. Physiological time-series analysis using approximate entropy and sample entropy. *American Journal of Physiology-heart and Circulatory Physiology*, 2000, **278**, H2039–H2049.